NAVAL POSTGRADUATE SCHOOL

MONTEREY, CALIFORNIA

THESIS

HIGHLY ABSORBING METAL NANOLAMINATES FOR Bi-MATERIAL THz SENSORS

by

Karamitros Apostolos

September 2011

Thesis Advisor:	Gamani Karunasiri
Co-Advisors:	David Jenn
	Dragoslav Grbovic

Approved for public release; distribution is unlimited

THIS PAGE INTENTIONALLY LEFT BLANK

REPORT DOCUMENTATION PAGE		Form Approved OMB No. 0704-0188
Public reporting burden for this collection of information is estimated to average 1 hour per response, including the time for reviewing instruction, searching existing data sources, gathering and maintaining the data needed, and completing and reviewing the collection of information. Send comments regarding this burden estimate or any other aspect of this collection of information, including suggestions for reducing this burden, to Washington headquarters Services, Directorate for Information Operations and Reports, 1215 Jefferson Davis Highway, Suite 1204, Arlington, VA 22202-4302, and to the Office of Management and Budget, Paperwork Reduction Project (0704-0188) Washington DC 20503.		
1. AGENCY USE ONLY ***(Leave blank)***	**2.REPORT DATE** September 2011	**3. REPORT TYPE AND DATES COVERED** Master's Thesis
4. TITLE AND SUBTITLE Highly Absorbing Metal Nanolaminates for Bi-Material THz Sensors		**5. FUNDING NUMBERS**
6. AUTHOR(S) Karamitros Apostolos		
7. PERFORMING ORGANIZATION NAME(S) AND ADDRESS(ES) Naval Postgraduate School Monterey, CA 93943-5000		**8. PERFORMING ORGANIZATION REPORT NUMBER**
9. SPONSORING /MONITORING AGENCY NAME(S) AND ADDRESS(ES) N/A		**10.SPONSORING/MONITORING AGENCY REPORT NUMBER**
11. SUPPLEMENTARY NOTES The views expressed in this thesis are those of the author and do not reflect the official policy or position of the Department of Defense or the U.S. Government. IRB Protocol number: N/A.		
12a. DISTRIBUTION / AVAILABILITY STATEMENT Approved for public release; distribution is unlimited		**12b. DISTRIBUTION CODE**

13. ABSTRACT (maximum 200 words)

The terahertz (THz) region of the electromagnetic spectrum covers frequencies ranging from approximately 100 GHz to 10 THz. This region of the spectrum has not been fully utilized due to the lack of compact and efficient sources as well as detectors.

The aim of the present research is to explore the use of thin metal films as high THz absorbing materials and determine their absorbing characteristics in the THz range both analytically as well as experimentally. These films are to be used in bi-material-based suspended structures which sense minute changes in temperature due to THz absorption via difference in thermal expansion coefficients in materials used in the structures. Nickel thin films with thicknesses ranging from 3 to 50 nm were deposited on silicon substrates using e-beam evaporation and were characterized using Fourier transform infrared (FTIR) spectroscopy extended to the THz range. Calculating Fresnel's transmission and reflection coefficient allowed us to theoretically predict the absorption of the films which was found to agree well with the measurements.

Further numerical analysis of absorption as a function of Ni film thickness indicates that the maximum possible value of absorption is 50%. This is experimentally demonstrated using a 2.9 nm Ni film. In addition, it is found analytically that for a given conductivity there is a unique thickness that gives the highest possible absorption (50%). This is highly significant since it allows us to explore the use of other potential metal thin films as well as doped semiconductors as THz absorbers for integration into bi-material sensors.

14. SUBJECT TERMS Bi-material structure, Nickel Thin films, Terahertz Absorption, Fresnel's Equations, FTIR Spectroscopy, maximizing the THz absorption			**15. NUMBER OF PAGES** 65
			16. PRICE CODE
17. SECURITY CLASSIFICATION OF REPORT Unclassified	**18. SECURITY CLASSIFICATION OF THIS PAGE** Unclassified	**19. SECURITY CLASSIFICATION OF ABSTRACT** Unclassified	**20. LIMITATION OF ABSTRACT** UU

THIS PAGE INTENTIONALLY LEFT BLANK

Approved for public release; distribution is unlimited

HIGHLY ABSORBING METAL NANOLAMINATES FOR Bi-MATERIAL THz SENSORS

Karamitros Apostolos
Lieutenant Junior Grade, Greek Navy
B.S., Hellenic Naval Academy, 2004

Submitted in partial fulfillment of the
requirements for the degrees of

MASTER OF SCIENCE IN ELECTRONIC WARFARE SYSTEMS ENGINEERING
and
MASTER OF SCIENCE IN ELECTRICAL ENGINEERING

from the

NAVAL POSTGRADUATE SCHOOL
September 2011

Author: Karamitros Apostolos

Approved by: Gamani Karunasiri
Thesis Advisor

Dragoslav Grbovic
Co-Advisor

David Jenn
Co-Advisor

Dan C. Boger
Chair, Department of Information Science

R. Clark Robertson
Chair, Department of Electrical and Computer Engineering

THIS PAGE INTENTIONALLY LEFT BLANK

ABSTRACT

The terahertz (THz) region of the electromagnetic spectrum covers frequencies ranging from approximately 100 GHz to 10 THz. This region of the spectrum has not been fully utilized due to the lack of compact and efficient sources as well as detectors.

The aim of the present research is to explore the use of thin metal films as high THz absorbing materials and determine their absorbing characteristics in the THz range both analytically as well as experimentally. These films are to be used in bi-material-based suspended structures which sense minute changes in temperature due to THz absorption via difference in thermal expansion coefficients in materials used in the structures. Nickel thin films with thicknesses ranging from 3 to 50 nm were deposited on silicon substrates using e-beam evaporation and were characterized using Fourier transform infrared (FTIR) spectroscopy extended to the THz range. Calculating Fresnel's transmission and reflection coefficient allowed us to theoretically predict the absorption of the films, which was found to agree well with the measurements.

Further numerical analysis of absorption as a function of Ni film thickness indicates that the maximum possible value of absorption is 50%. This is experimentally demonstrated using a 2.9 nm Ni film. In addition, it is found analytically that for a given conductivity there is a unique thickness that gives the highest possible absorption (50%). This is highly significant since it allows us to explore the use of other potential metal thin films as well as doped semiconductors as THz absorbers for integration into bi-material sensors.

THIS PAGE INTENTIONALLY LEFT BLANK

TABLE OF CONTENTS

THIS PAGE INTENTIONALLY LEFT BLANK

LIST OF FIGURES

LIST OF TABLES

THIS PAGE INTENTIONALLY LEFT BLANK

LIST OF ACRONYMS AND ABBREVIATIONS

Cr	Chromium
FPA	Focal Plane Array
FTIR	Fourier Transform Infrared
IR	Infrared
MEMS	Microelectromechanical Systems
Ni	Nickel
ONR	Office of Naval Research
QCL	Quantum Cascade Laser
SNR	Signal-to-Noise Ratio
THz	Terahertz

THIS PAGE INTENTIONALLY LEFT BLANK

EXECUTIVE SUMMARY

There is a renewed interest in the terahertz (THz) frequency range (100 GHz to 10 THz) for imaging applications due to its potential for identification of concealed weapons, quality control in manufacturing, medical imaging and inspection of fragile artwork.

Real-time imaging in the THz spectral range has been achieved using an uncooled microbolometer infrared (IR) camera and a milliwatt-scale quantum cascade laser (QCL) as an illuminator. The principle of radiation detection is based on temperature changes arising from the absorption of THz waves by an absorbing layer within the camera pixel. The disadvantage of this scheme is that bias used for reading the resistance change generates heat (self-heating) in the pixel, which limits the integration time, affecting the signal-to-noise ratio. On the other hand, an alternative and more efficient readout technique is under development. This involves deformation of a bi-material based suspended structure by minute changes in temperature due to difference in thermal expansion coefficients of layers of material used to build the pixel.

The use of micro-electro-mechanical system (MEMS) based bi-material sensors allows the implementation of an optical readout process, which can result in a better signal-to-noise ratio. In addition, it can avoid the integration of readout electronics, resulting in a simplified fabrication process. For improving the sensitivity of bi-material pixels for THz imaging, it is necessary to develop high THz absorbing thin films.

The identification of nanoscale thin metal films with optimal absorption between 1 to 10 THz to be integrated in imaging sensors is the focus of this thesis. One of the potential candidates is nickel (Ni), which is compatible with MEMS fabrication process and has less residual stress when integrated with the bi-material pixel. Transmission and reflection coefficients are calculated using Fresnel's equations, which allow theoretical prediction of absorption in films. Further analysis of absorption as a function of Ni film thickness indicates that the maximum possible value of absorption is 50%. For determining absorption as a function of film thickness, Ni thin films with thicknesses ranging from 3 to 50 nm were deposited on silicon substrates using e-beam evaporation.

The transmission (T) and reflection (R) coefficients of the samples were measured using a Fourier transform infrared (FTIR) spectrometer extended to the THz range.

The absorption (A) of each sample is determined using $A = 1 - T - R$. The experimental absorption as a function of THz frequency shows good agreement with that of the calculated spectra, and the 2.9 nm Ni film measured 48%, close to the theoretically predicted value. This is significant since it allows us to explore the use of other potential metal thin films as well as doped semiconductors as THz absorbers for integrating with bi-material sensors.

ACKNOWLEDGMENTS

I would like to thank Professor Gamani Karunasiri, Professor Dragoslav Grbovic and Professor David Jenn for all their guidance during the course of this research and throughout my graduate studies. Their support and advice was direct and inspiring. Moreover, I would like to thank Dr. Fabio Alves for providing me professional directions and helping me to finalize this research. This work is supported in part by a grant from the Office of Naval Research (ONR) and the National Reconnaissance Office (NRO).

THIS PAGE INTENTIONALLY LEFT BLANK

I. INTRODUCTION

A. OVERVIEW

Terahertz imaging has seen significant proliferation in recent years. This band of the electromagnetic spectrum (100 GHz to 10 THz) has been underutilized for a long time due to the lack of sufficiently powerful sources and sensitive detectors. Its non-ionizing nature renders THz radiation effects virtually harmless to living tissue, and its property of being able to penetrate most insulating materials (textiles, paper, etc.) while reflecting from metallic objects makes it a good candidate for the leading role in applications involving detection of concealed objects and medical imaging. To name a few applications, in the area of homeland security, THz imagers can be used to detect concealed metal objects or certain types of explosives due to their characteristic THz signatures. Moreover, in the field of medicine, THz imaging appears particularly suited for examining skin abnormalities such as skin cancer and characterizing human tissues [1, 2].

For the reasons mentioned above, there is now interest in fabricating detector arrays operating in the THz frequency band. In a recent experiment, real-time THz imaging was successfully demonstrated using a conventional uncooled microbolometer infrared camera fitted with THz optics [3, 4]. The camera was originally designed to operate in the 7–13 μm wavelength band and has a temperature resolution of about 60 mK. The sensitivity of thermal cameras is strongly dependent on the absorbing material used as the pixel membrane. Imaging using the camera, however, required a milliwatt-scale 2.8 THz quantum cascade laser (QCL) to act as an illuminator due to the lack of appreciable THz radiation in the 300 K background [4, 5].

The optimization of the microbolometer focal plane array (FPA) for THz detection requires a change in pixel size (due to a longer wavelength) and integration of readout electronics, which was relatively complex and expensive. The new approach to overcome these difficulties is to incorporate micro-electro-mechanical systems (MEMS) based bi-material detectors [6]. The approach described in [6] for the detection of THz

using a bi-material pixel involves deflection of a suspended bi-material structure to minute changes in temperature due to absorption of THz radiation. This implies that, for achieving high sensitivity, it is important to develop a strong THz absorbing membrane to integrate onto the pixel.

Towards achieving this goal, the use of nanosacale metal films for THz absorption was theoretically analyzed with the help of Fresnel's equations. The aim was to develop a model that can estimate the absorption properties of a multilayer stack in the THz region and be used to maximize the absorption of THz radiation. Previous efforts have also used various models for optimizing the thickness of the Chromium (Cr) layer for achieving strong THz absorption. It was found that a Cr layer of approximately 10 nm achieves nearly 50% absorption of incident THz power [7, 8].

B. OBJECTIVE

The aim of the research is to develop high THz absorbing nanoscale thin films to be integrated with MEMS bi-materials sensors. The pixel architecture shown in Figure 1 undergoes a deformation due to absorption of THz radiation. This deformation is achieved by designing the detector to have areas of bi-material layers. The bi-material layers usually consist of a structural layer coated with a metal film having different coefficient of thermal expansion to that of the structural layer. When the detector temperature increases, these two layers expand at different rates, causing the whole structure to deform. Having high sensitivity in mind, it is expected that this type of detector would be appropriate for detection of THz radiation [7], and it is important to develop a strong THz absorbing membrane to integrate into the pixel.

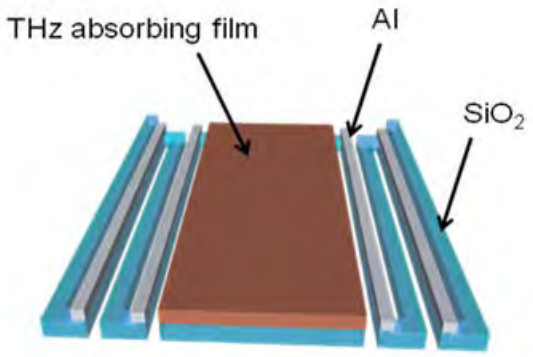

Figure 1. Schematic of a bi-material pixel with mechanical amplification (using a folded leg structure) for THz sensing (From [5]).

In a previous study [7], a model for Cr metal films was developed to assess the absorption characteristics of the films. It could be generalized to any metal layer of known conductivity. The focus of this thesis is to identify nanoscale thin films with optimal absorption between 1 to 10 THz that can be integrated into imaging sensors. During the initial stage, the absorption characteristics are to be analyzed theoretically to determine the optimum thickness range for fabrication. The fabricated films are to be characterized using a Fourier transform infrared (FTIR) spectrometer extended to the THz range to determine the absorption as a function of film thickness.

C. THESIS OUTLINE

This thesis is organized as follows. The importance of the research is outlined in Chapter I, and previous efforts are briefly summarized. In Chapter II, the fundamentals of the FTIR spectroscopy are presented in order to understand the tools that are needed for experimental measurements. In Chapter III, The theoretical analysis of THz absorption of thin films is provided. The experimental and theoretical simulation results are compared in Chapter IV. In Chapter VI, a new bi-material structure model is presented. Finally, in Chapter V, the conclusions of this research are presented.

THIS PAGE INTENTIONALLY LEFT BLANK

II. FUNDAMENTALS OF FTIR SPECTROSCOPY

In this chapter, the fundamental measurement of transmission and reflection using spectroscopy is described.

A. GENERAL DESCRIPTION OF FTIR

Fourier transform infrared spectroscopy is a technique used to obtain infrared spectral characteristics (transmission and reflection) of a sample. An FTIR spectrometer consists of a Michelson interferometer with a moving mirror. It collects spectral information for a sample simultaneously for all the wavelengths using a broadband thermal source. The resulting signal, which is called the interferogram, is the Fourier transform of the spectral information [4]. The interferogram data is processed by inverse Fourier transformation to extract the spectral information as a function of wavelength [9]. During this work, a Thermo Fisher NEXUS 870 FTIR was used to measure transmission and reflection coefficients from which the absorption of the nickel thin films was estimated. The spectrometer is capable of measuring the THz radiation transmitted through the sample or the radiation reflected by using two gold mirrors to steer the beam. The data is corrected by subtracting the background data taken without the sample to eliminate non-uniform spectral characteristics of the spectrometer at different wavelengths.

B. THEORY OF INFRARED SPECTROSCOPY

Fourier transform infrared is the preferred method of infrared spectroscopy. An FTIR consists of a Michelson Interferometer [9] with one fixed mirror and a moving mirror for scanning, as illustrated in Figure 2. The light from a broadband source (heated filament) hits the beamsplitter, and one half goes to the fixed mirror while another half goes to the moving mirror. The beamsplitter then gathers the reflected light from each mirror and recombines it so that can be led through the sample to the detector [9].

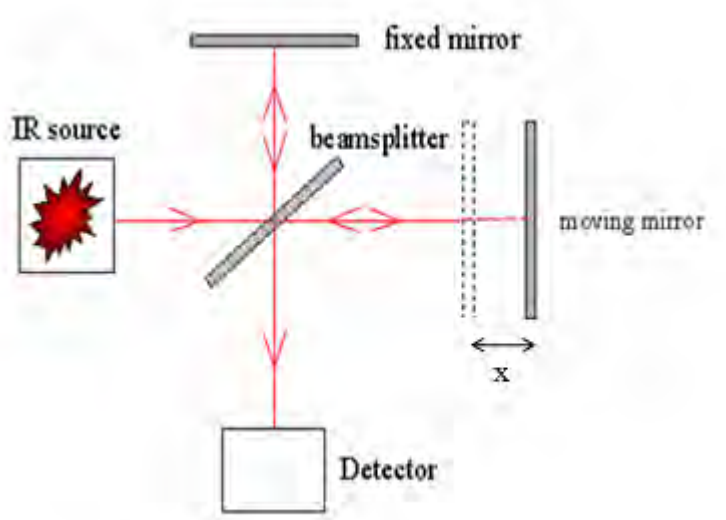

Figure 2. Schematic diagram of a Michelson interferometer used in FTIR spectrometer (From [9]).

The electric field of an incoming monochromatic plane wave can be written as

$$\vec{E} = \vec{E}_m \cos(\omega t - 2\pi kx) \tag{1}$$

where ω is the radian frequency, $k = 1/\lambda$ cm^{-1} is the modified wavenumber, λ is the wavelength and x is the displacement of the moving mirror from the location where the two mirrors are equal distance from the beamsplitter. The vector $\vec{E}_m$ defines the polarization and the amplitude at the reference position.

The detected intensity *I(x)* as a function of the translating mirror's displacement x is given by [9]

$$I(x) = I(k)[1 + \cos(2\pi kx)] \tag{2}$$

where *I(k)* is the intensity of the source at wavenumber k. For a broadband source, the intensity at the detector is determined by integrating Equation (2) over all wavenumbers. Then *I(k)* can be determined by taking inverse Fourier transform of the detected intensity as a function of the modified wavenumber k as [9]

$$I(k) = \int_0^{\infty} \left[I(x) - \frac{I(0)}{2} \right] \cos(2\pi kx) dx \,. \tag{3}$$

The software Omnic, which is provided with the NEXUS 870 FTIR, does the analysis and produces the spectral information.

C. BASIC FTIR SPECTROMETER PARAMETERS USED

Before starting the experimental measurements, the adjustment of some basic parameters of the FTIR, such as the gain, resolution, number of scans and velocity of the moving mirror, are necessary [10]. The default setting for the gain is the autogain. In order to avoid saturation of the detector, the adjustment of parameters has to be performed carefully. The resolution has to do with how sharper spectral features in the spectrum can be resolved. The default setting for the resolution in wavenumbers is 4 cm^{-1}, which corresponds to an average data spacing of 2 cm^{-1}. The number of scans in combination with the velocity of the moving mirror can be adjusted improve the signal-to-noise ratio. The settings used for the number of scans and mirror's velocity were 128 and 0.1583 m/s, respectively.

In this chapter, the spectroscopy measurement technology and parameters have been presented. The analytical approach to predicting transmission and reflection from multiple layers are discussed in Chapter III.

THIS PAGE INTENTIONALLY LEFT BLANK

III. MODELING AND CHARACTERIZATION

A. THEORETICAL BACKGROUND

The power transmission and reflection coefficients of thin metal films are calculated using Fresnel's equation, which also allows the prediction of absorption [7]. The fractional absorption is estimated by subtracting the two coefficients from unity. Let us consider an arbitrary three layers inside of a stack as depicted in Figure 3, where n_i represents the index of refraction, e_i the thickness and θ_i the angle of incidence for the i^{th} layer, respectively.

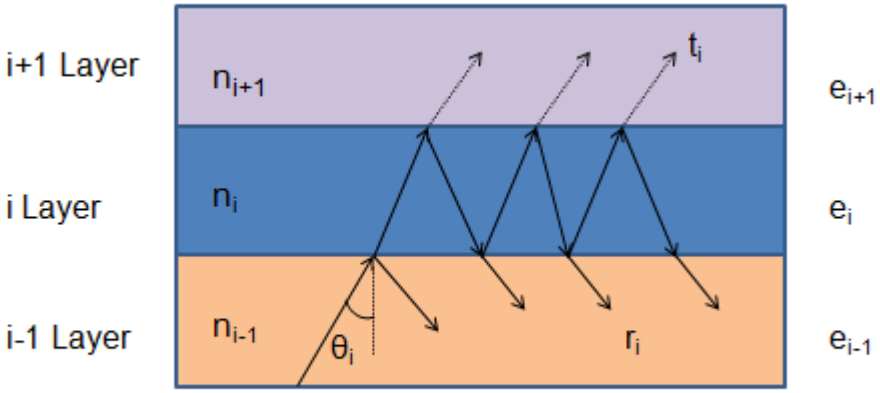

Figure 3. Three layer stack used for the calculation of reflection and transmission coefficients.

The boundary conditions at the interfaces allow the Snell's law of refraction to be derived as

$$n_{i-1}\sin\theta_{i-1} = n_i \sin\theta_i = n_{i+1}\sin\theta_{i+1}. \quad (4)$$

The effective reflection (r_i) and transmission (t_i) coefficients between the i^{th} and the $i+1^{th}$ interface can be obtained by summing the multiple transmissions and reflections occurring at i^{th} layer as [11, 12]

$$r_i = \frac{r_{i-1,i} + r_{i,i+1} e^{-2j\varphi_i}}{1 + r_{i\text{-}1,i} r_{i,i+1} e^{-2j\varphi_i}} \tag{5}$$

where the reflection coefficients $r_{i,i+1}$ are given by the standard Fresnel formulas [11] applied to the boundary between layers i and $i+1$, r_i is the sum of the multiple reflected beams and φ_i is the change in phase when propagating through layer i. The phase change is given by

$$\phi_i = \frac{2\pi}{\lambda} n_i e_i \cos\theta_i . \tag{6}$$

Similarly, for the effective transmission coefficient,

$$t_i = \frac{t_{i-1,i} t_{i,i+1} e^{-j\varphi_i}}{1 + r_{i\text{-}1,i} r_{i,i+1} e^{-2j\varphi_i}} \tag{7}$$

where t_i is the sum of the multiple transmitted beams and $t_{i,i+1}$ the Fresnel coefficients of transmission for interface between i^{th} and $i+1^{th}$ layer, respectively [11].

For a single layer, assuming the first and the last layers to be air, the counter takes on only one value, i=2. Based on the Rouard method [11], this approach can be generalized for a stack containing an arbitrary number of films.

In order to obtain the total reflection (fraction of the incoming power reflected) and transmission (fraction of the incoming power transmitted) coefficients as a function of THz frequency for the nickel thin films, a computer program was developed [7] (as described in Appendices A and B). The index of refraction for the metal is [12]

$$n_{metal} = (1 - j)\sqrt{\frac{1}{4\pi\varepsilon_o c}}\sqrt{\sigma\lambda} \tag{8}$$

where σ is the conductivity of the silicon substrate and λ is the wavelength of the incident radiation. The complex index of refraction for the Si substrate was calculated using [13]

$$n_{si} = \sqrt{\varepsilon_r} - j\frac{\sigma\lambda}{0.033\sqrt{\varepsilon_r}} \tag{9}$$

where σ is the conductivity of the silicon substrate and ε_r is the relative dielectric constant of silicon.

B. DESCRIPTION OF NICKEL THIN FILMS

Experimental measurements were carried out using twelve nickel thin films of different thicknesses. Note that at nanoscale thicknesses, as the film thickness decreases, the conductivity also decreases due to increase in surface scattering. Nickel films were deposited on 300, 450 or 500 μm silicon substrates using e-beam evaporation. Four of the samples included a multilayer stack with five layers of SiO_2 and Si_3Ni_4 having thicknesses of 110 nm and 75 nm, as shown in Figure 4 (a). The indices of refraction used for the SiO_2 and Si_3N_4 were 1.46 and 2.05, respectively. These dielectric layers act as a Bragg reflector for optical readout of bi-material pixels, which does not affect the absorption of Ni films. The rest of the nickel thin films were deposited directly on the silicon substrate without the multilayer stack (see Figure 4b).

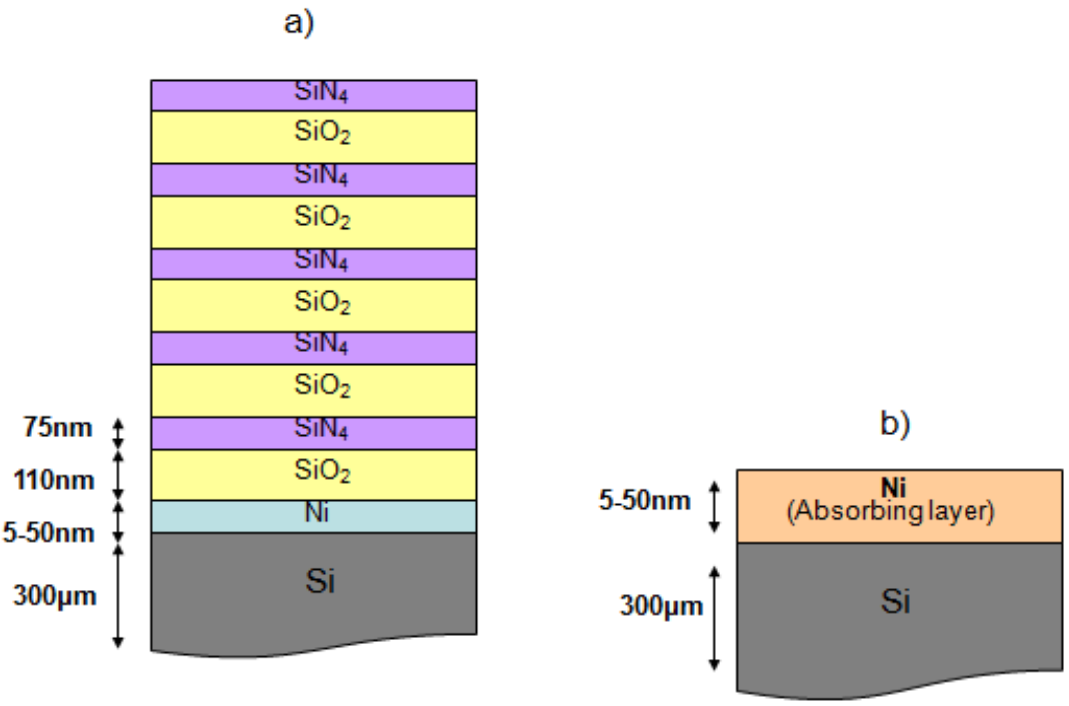

Figure 4. (a) Structure of the samples with Ni film and multilayer stack containing SiO_2 and Si_3Ni_4 layers and (b) structure of samples with Ni thin films deposited directly on silicon substrate.

The measured thicknesses using a surface profiler and conductivities using a four-point probe of the Ni layers are listed in Table 1. Moreover, the conductivities of the Si substrates were also measured and are given in Table 2.

Table 1. Thickness and conductivities values for the wafers used for deposition of Ni (From [14]).

Sample N_o	**Thickness (nm)**	**Conductivity S/m**	**Layers of SiO_2 and Si_3Ni_4**
1	3	1.8×10^6	No
2	6.5	2.77×10^6	No
3	8	3.22×10^6	No
4	10	3.33×10^6	No
5	15	4×10^6	No
6	18	4.54×10^6	No
7	20	4.34×10^6	No
8	50	8.33×10^6	No
9	10	4×10^6	Yes
10	15	3.57×10^6	Yes
11	20	4.34×10^6	Yes
12	30	4.54×10^6	Yes

Table 2. Conductivities and thicknesses of Si substrates used for the preparation of samples (From [14]).

Sample No	**Conductivity (S/m)**	**Substrate Thickness (μm)**
1	7×10^{-4}	485
2	6.4×10^{-4}	500
3	4.7×10^{-4}	500
4	8.695	300
5	6.25	300
6	4.3478	300
7	9.0909	300
8	6.6	450
9	6.25	300
10	5.555	300
11	3.846	300
12	9.0909	300

Using the equations for transmission and reflection coefficients, we calculated the absorption of the samples for frequencies from 2.5 to 10 THz at an angle of incidence of 30 degrees (for the reason that will be discussed in the following sections). Figures 5, 6 and 7 are plots of the calculated reflection, transmission and absorption spectra, respectively, for the 10 nm thick Ni film (sample # 1). The oscillations in the spectra are due to the Fabry-Perot effect associated with reflection of THz from the front and backsides of the 300 μm Si substrate.

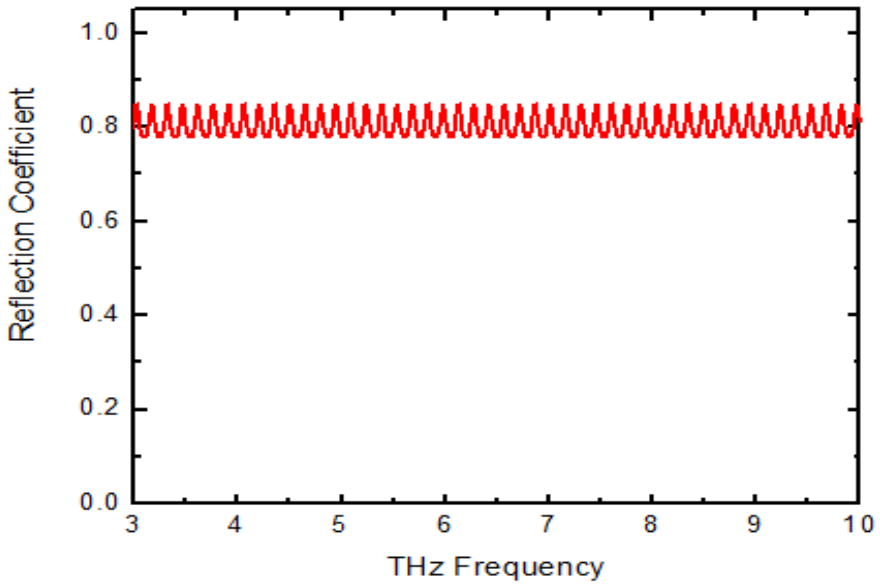

Figure 5. Calculated reflection coefficient of Ni thin film with 10 nm thickness as a function of THz frequency.

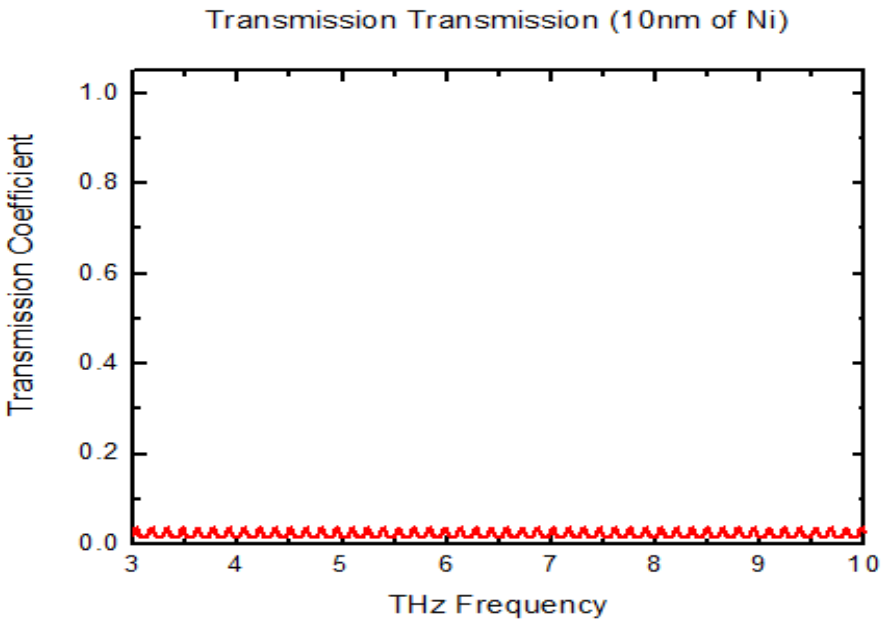

Figure 6. Calculated transmission coefficient of Ni thin film with 10 nm thickness as a function of THz frequency.

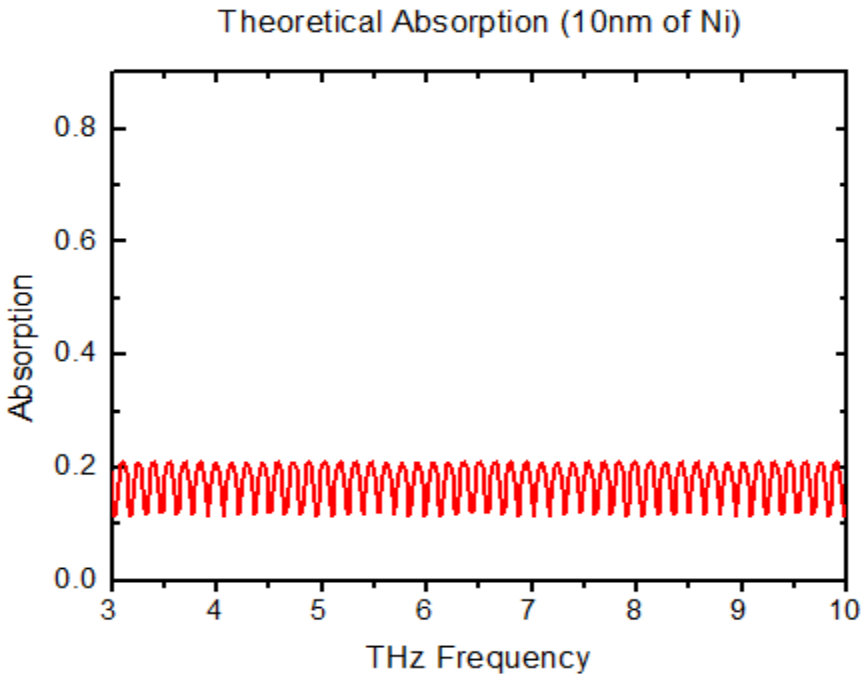

Figure 7. Calculated absorption of Ni thin film with 10 nm thickness as a function of THz frequency.

C. MEASUREMENT OF TRANSMISSION COEFFICIENT

The experimental setup for measuring the transmission through a wafer is shown schematically in Figure 8. In order to perform this measurement, the desired wafer was placed in the sample compartment of the FTIR as depicted in Figure 9. The reflection measurement had to be taken at off-normal incidence (30°) using an arrangement of two gold mirrors to steer the FTIR beam, as will explained in the following section. Because of this, the transmission coefficient was also measured by placing the sample at 30 degrees to the incident beam from the spectrometer. After measuring the transmission spectrum of the sample, we also collected the background spectrum by removing the sample to correct the non-uniform spectral characteristics of the FTIR as discussed in Chapter I. Since the theoretical model gave low transmission for the sample, the speed of the moving mirror of the FTIR was reduced to increase the beam throughput for attaining higher signal-to-noise ratio. The remaining measurement parameters were left at the default values.

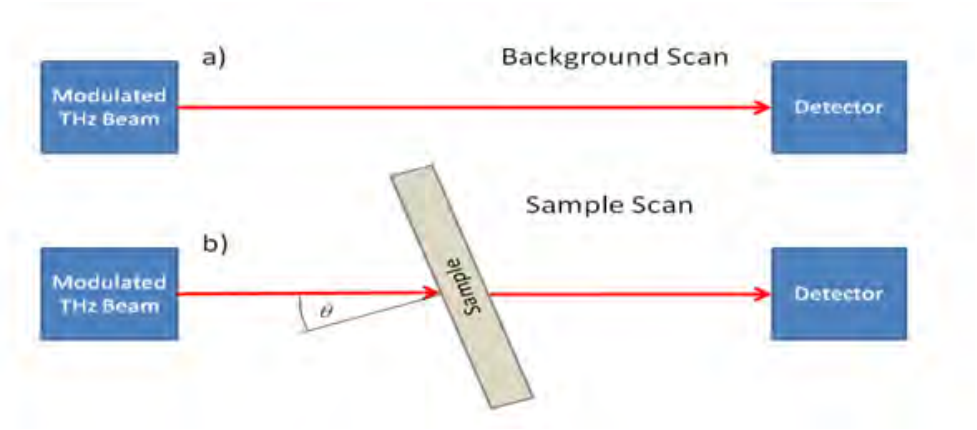

Figure 8. Schematic of the experimental setup used to collect (a) the background and (b) sample for determining transmission coefficient (From [7]).

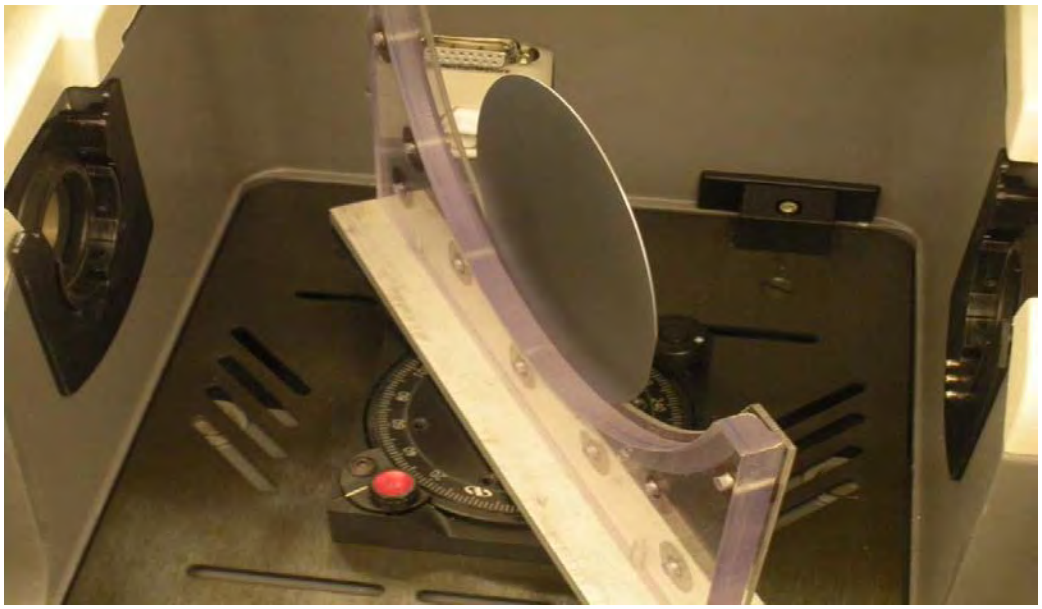

Figure 9. Sample compartment of FTIR showing the placement of the sample in the transmission measurement.

Measured transmission coefficient of the sample with 10 nm Ni layer as a function of THz frequency is depicted in Figure 10.

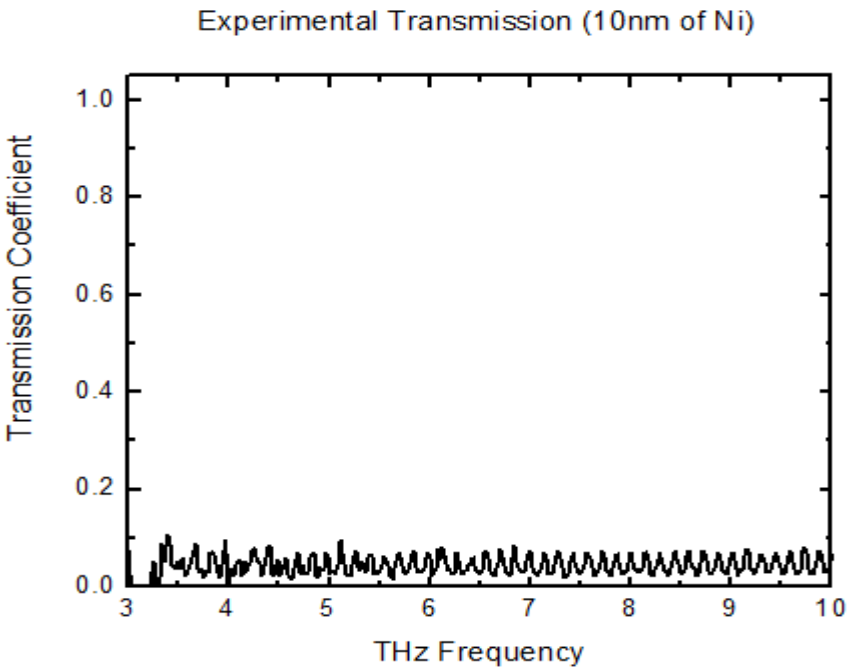

Figure 10. Measured transmission coefficient of 10 nm Ni as a function of THz frequency.

D. MEASUREMENT OF REFLECTION COEFFICIENT

Schematics of the measurement approach to measuring the reflection coefficient are illustrated in Figure 11. Two gold mirrors were placed on a base as shown with an angle of 60 degrees with respect to their axis of symmetry. In this way, the reflected beam of the FTIR is guided towards the FTIR detector with a 30-degree angle of incidence. In order to measure the background, a gold coated silicon wafer, which behaves as a perfect mirror with reflection close to 100%, was used. The experimental arrangement used for the reflection measurement in the sample compartment of the FTIR is shown in Figure 12.

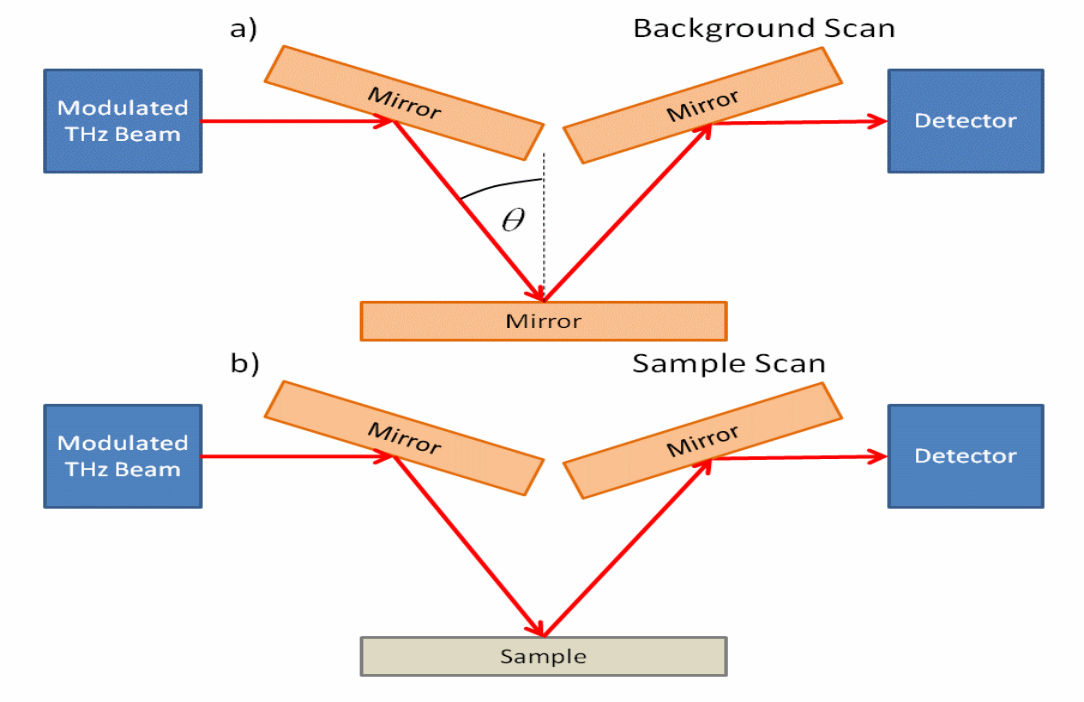

Figure 11. Schematic of the experimental setup used to collect (a) the background and (b) sample for determining reflection coefficient (From [7]).

Figure 12. Sample compartment of FTIR showing the placement of the sample in the reflection measurement.

The measured reflection coefficient of the sample with 10 nm Ni layer as a function of frequency is shown in Figure 13.

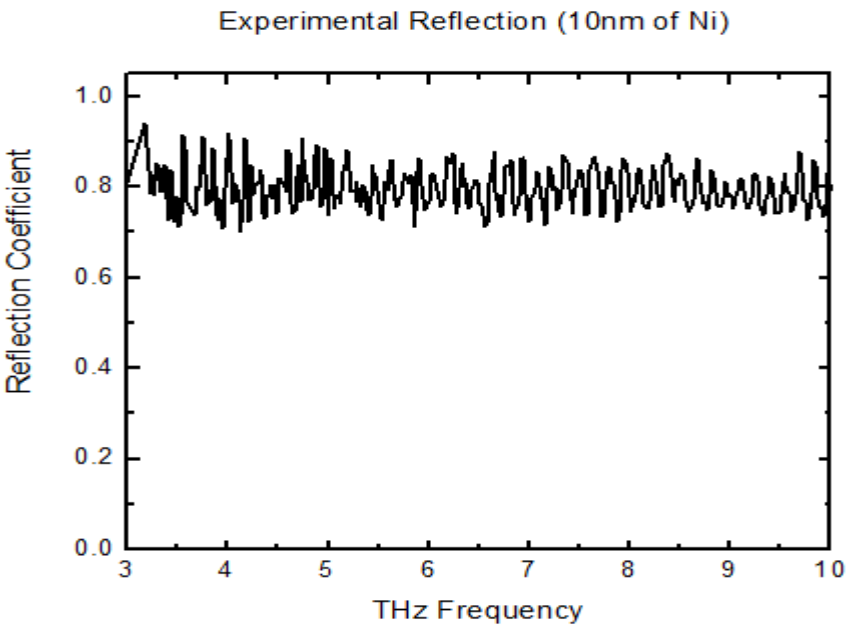

Figure 13. Experimental reflection of the thin film of 10 nm of Ni as a function of THz frequency.

E. DETERMINATION OF ABSORPTION

In order to determine the experimental absorption of the nickel thin films, we subtract the sum of reflection and transmission coefficients from one at each frequency. The respective experimental results for the absorption of the 10 nm of nickel as a function of frequency are shown in Figure 14.

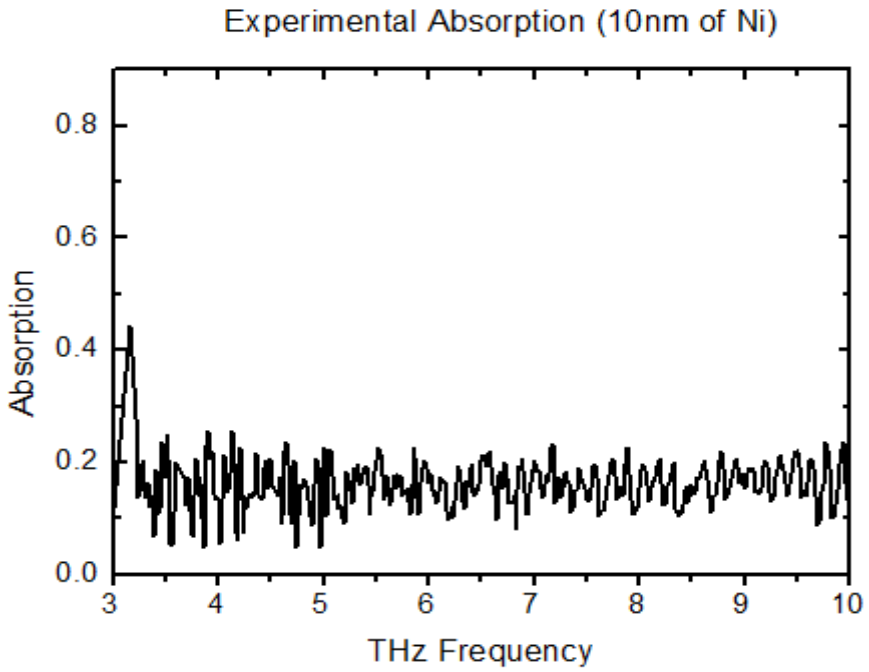

Figure 14. Experimental absorption of thin film with 10 nm Ni layer as a function of THz frequency.

This procedure was repeated for all the 12 samples to obtain the absorption spectra. A comparison of the measured and calculated absorption spectra will be presented in the next chapter.

IV. DISCUSSION

A. COMPARISON OF SIMULATION AND EXPERIMENTAL RESULTS

Comparisons of the experimental transmission, reflection and absorption spectra with these of the simulations (using MATLAB) for the 10 nm thick Ni sample are shown in Figures 15 to 17, respectively. The measured spectra show good correlation with the simulation, indicating the accuracy of the theoretical analysis. As can be seen for the 10 nm sample (Figure 17), the absorption reaches approximately 21% [15]. To clearly see the close agreement between measurement and simulation, a narrow spectral band (9-10 THz) is plotted in Figure 18.

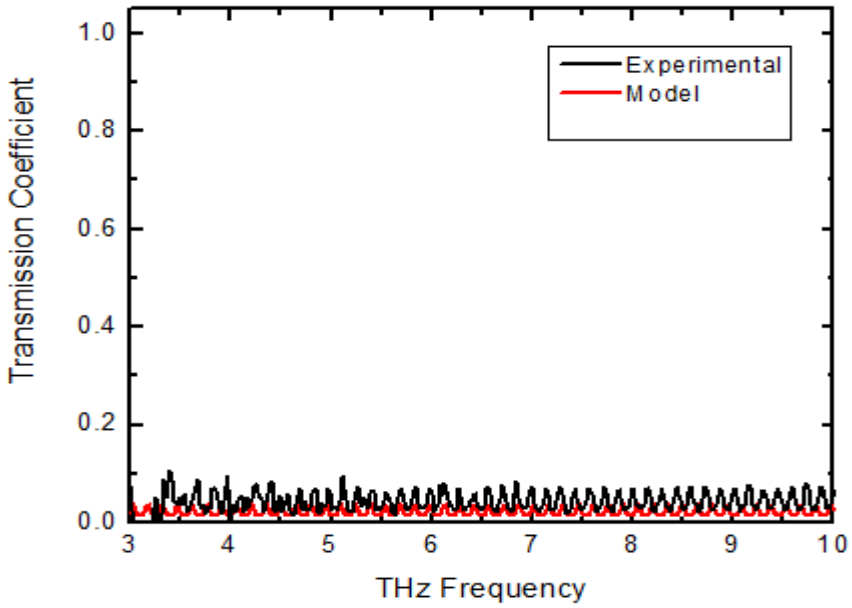

Figure 15. Experimental versus simulated transmission coefficient of 10 nm Ni layer as a function of THz frequency.

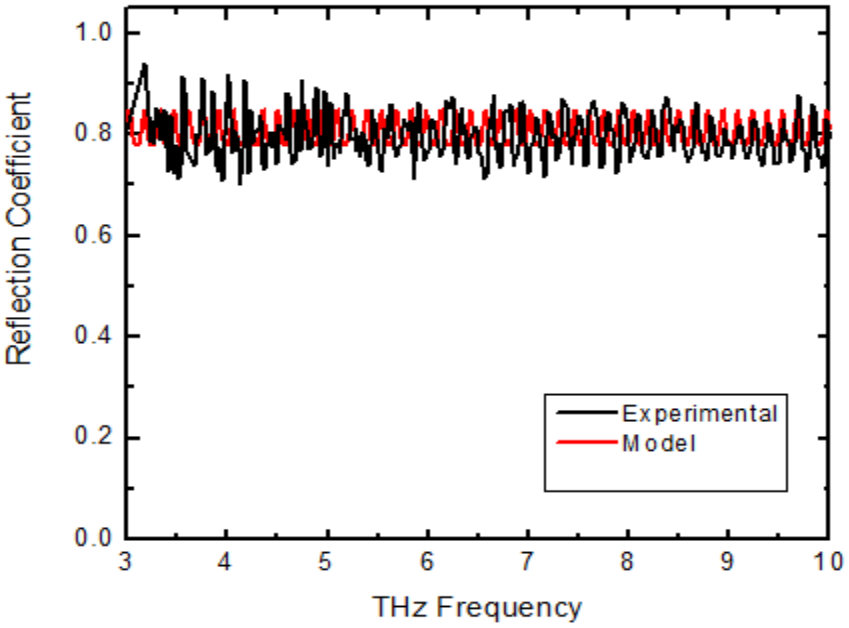

Figure 16. Experimental versus simulated reflection coefficient of 10 nm Ni layer as a function of THz frequency.

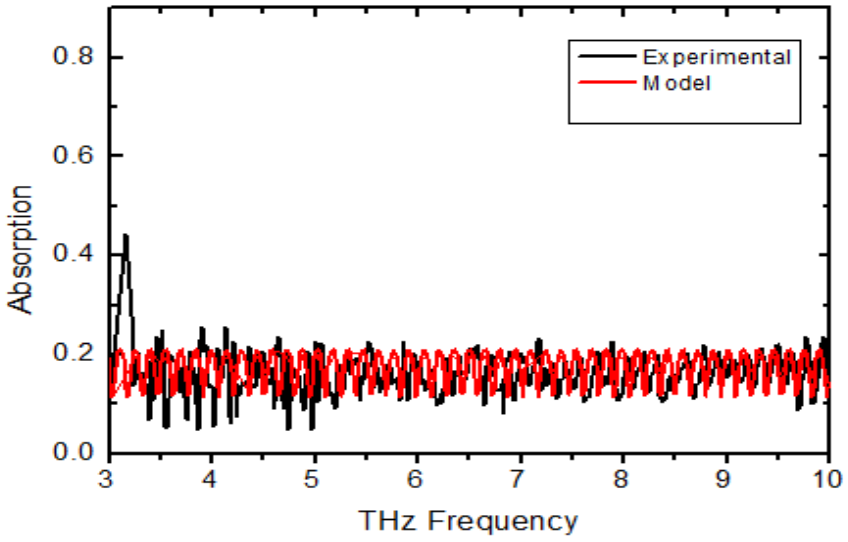

Figure 17. Experimental versus simulated absorption of 10 nm Ni layer as a function of THz frequency.

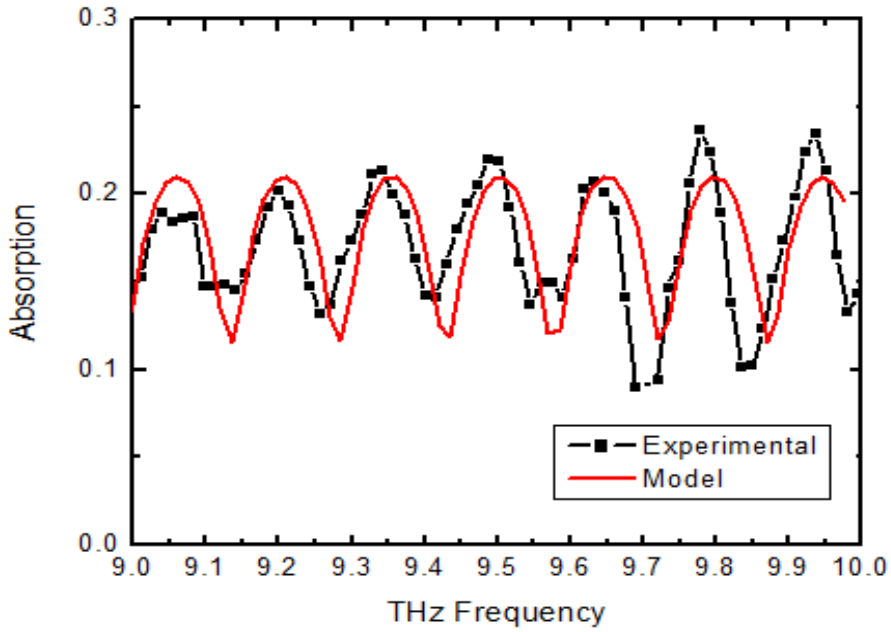

Figure 18. Comparison of modeled and experimental values for 10 nm Ni film in 9-10 the THz range.

B. ABSORPTION IN SUBSTRATE

In order to determine the contribution from the substrate relative to the total absorption of the samples, the reflection and transmission coefficients were measured for a blank silicon wafer of 300 μm thick and conductivity of 0.0625 S/m. The estimated absorption based on the measurement along with that of the simulated spectrum in the 3–5 THz range is shown in Figure 19. The absorption by the substrate is close to 30%. The oscillation is as expected and arises from the Fabry-Perot effect due to reflection between front and back surfaces of the wafer.

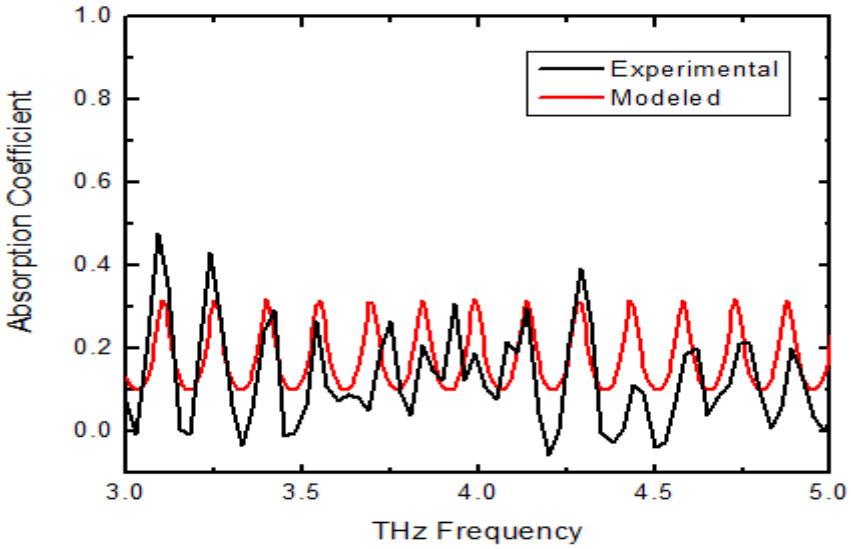

Figure 19. Experimental and simulated absorption of the blank wafer as a function of THz frequency.

C. DATA ANALYSIS

When thin films are grown on a thick substrate, the absorption shows fringes due to the Fabry-Perot effect, which makes the determination of the absorption the film difficult. However, these films are employed in the THz bi-material pixels using a very thin (1 μm) supporting dielectric layer. The use of such a thin layer practically eliminates the fringes in the THz range of interest due to the long wavelengths involved (100 μm). It is important to extract the absorption of the film without the substrate. In Figure 20, the simulated absorption spectrum for the 10 nm thick nickel film is seen with and without the substrate. It is interesting to note that the absorption of the film without the substrate is independent of frequency and rides on the peaks of the absorption with substrate. Thus, in the subsequent analysis, the peak value of measured data is taken as the absorption of the film without the substrate [14].

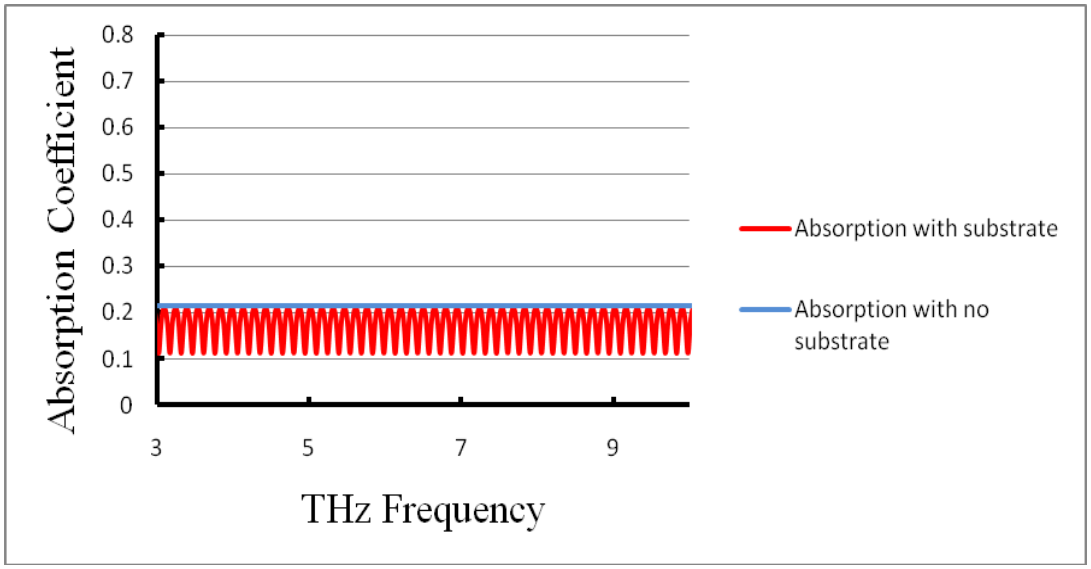

Figure 20. Simulated absorption of with 10 nm thick Ni layer with and without the substrate as a function of THz frequency. The conductivity of the film was taken to be 3.33×10^6 S/m.

Measured and simulated values of transmission, reflection and absorption for the 12 nickel thin-film samples are provided in Table 3. Note that the data in Table 3 represent estimation of transmission, reflection and absorption after removing the contribution from the substrates. As described earlier, this was done by taking the peak values of both measured and simulated spectra.

Table 3. Comparison of the peak values for coefficients for the Ni samples of 3 to 50 nm between 2.5 and 10 THz.

Sample 1 (3 nm)	Transmission Coefficient (%)	Reflection Coefficient (%)	Absorption (%)
Experimental (peak value)	**26**	**26**	**48**
Modeled (peak value)	**20**	**30**	**50**
Sample 2 (6.5 nm)	Transmission Coefficient (%)	Reflection Coefficient (%)	Absorption (%)

Experimental (peak value)	**5.8**	**65**	**29.2**
Modeled (peak value)	**4.5**	**63**	**32.5**
Sample 3 (8 nm)	Transmission Coefficient (%)	Reflection Coefficient (%)	Absorption (%)
Experimental (peak value)	**0.5**	**76**	**23.5**
Modeled (peak value)	**1.7**	**74**	**24.3**
Sample 4 (10 nm)	Transmission Coefficient (%)	Reflection Coefficient (%)	Absorption (%)
Experimental (peak value)	**3**	**75**	**22**
Modeled (peak value)	**2**	**78**	**20**
Sample 5 (15 nm)	Transmission Coefficient (%)	Reflection Coefficient (%)	Absorption (%)
Experimental (peak value)	**1**	**88**	**11**
Modeled (peak value)	**0.5**	**87**	**12.5**
Sample 6 (18 nm)	Transmission Coefficient (%)	Reflection Coefficient (%)	Absorption (%)
Experimental (peak value)	**1**	**90**	**9**
Modeled (peak value)	**1**	**89**	**10**
Sample 7 (20 nm)	Transmission Coefficient (%)	Reflection Coefficient (%)	Absorption (%)
Experimental (peak value)	**0.5**	**91**	**8.5**

Modeled (peak value)	**1**	**89**	**10**
Sample 8 (50 nm)	Transmission Coefficient (%)	Reflection Coefficient (%)	Absorption (%)
Experimental (peak value)	**0.09**	**96**	**3.903**
Modeled (peak value)	**0.07**	**97**	**2.93**
Sample 9 (10 nm)	Transmission Coefficient (%)	Reflection Coefficient (%)	Absorption (%)
Experimental (peak value)	**1**	**80**	**19**
Modeled (peak value)	**0.5**	**80.7**	**18.8**
Sample 10 (15 nm)	Transmission Coefficient (%)	Reflection Coefficient (%)	Absorption (%)
Experimental (peak value)	**1**	**87**	**12**
Modeled (peak value)	**0.5**	**85**	**14.5**
Sample 11 (20 nm)	Transmission Coefficient (%)	Reflection Coefficient (%)	Absorption (%)
Experimental (peak value)	**0.9**	**92.1**	**7**
Modeled (peak value)	**0.7**	**89.3**	**10**
Sample 12 (30 nm)	Transmission Coefficient (%)	Reflection Coefficient (%)	Absorption (%)
Experimental (peak value)	**1**	**91**	**8**
Modeled (peak value)	**0.8**	**93.2**	**6**

As we can observe from Table 3, thicker films result in higher reflection coefficients. The change in the transmission coefficient is less than that of the reflection coefficient, so that thickness of the film affects reflection more than transmission. This is due to the increase in conductivity as the thickness is increased [15] because of less pronounced surface scattering of electrons in the metal (see Figure 21). Note that the increase of conductivity of Ni films reaches its bulk value of about 1.4×10^9 S/m when the films are relatively thick. For the range of thicknesses used in this research, the absorption decreases as the film thickness increases. Note that the 3 nm thick nickel film results in absorption of approximately 48%, whereas the absorption of 50 nm film is only 3.9%. The samples 7 and 11 (20 nm films with and without the dielectric stack) show nearly the same absorption, indicating the multilayer stack does not impact absorption of the film underneath. A comparison of measured and simulated absorption as a function of thickness of the Ni film is shown in Figure 22. The measured data shows good agreement with that of the simulations.

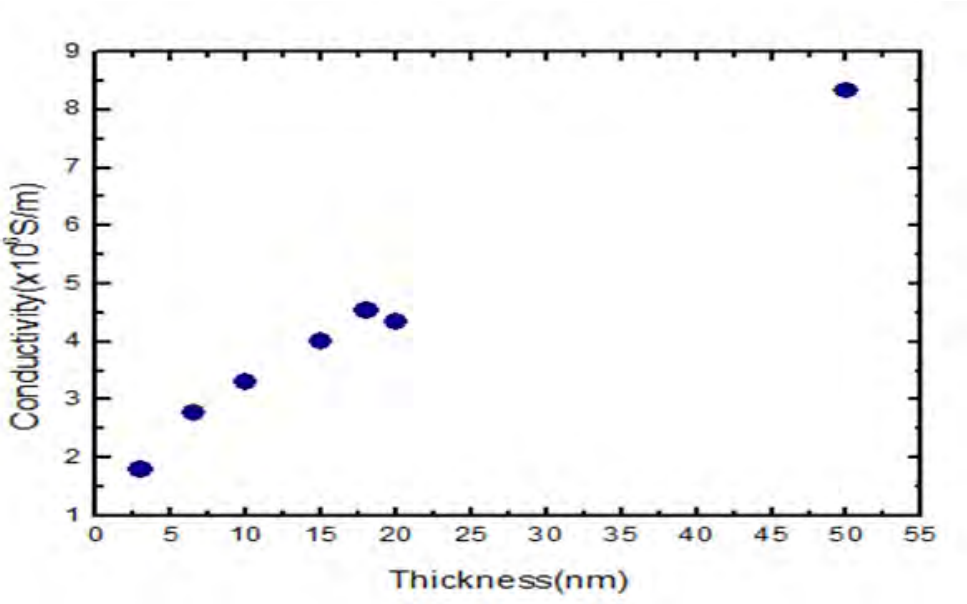

Figure 21. Dependence of conductivity and thickness.

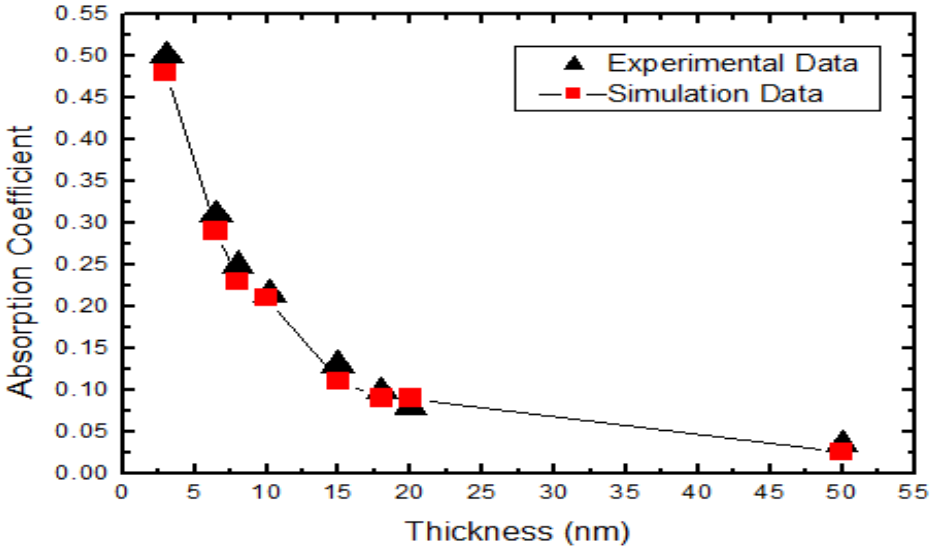

Figure 22. Experimental (black triangles) and simulated (red squares) absorption as a function of film thickness.

In the next chapter, a simulation model will be presented and discussed in order to determine the maximum absorption for nanoscale metal thin films for arbitrary values of thickness and conductivity.

THIS PAGE INTENTIONALLY LEFT BLANK

V. OPTIMIZATION OF ABSORPTION

In order to determine the maximum THz absorption possible using nanoscale metal films, the model described in Chapter III was extended for arbitrary combinations of thickness and conductivity.

A. DESCRIPTION OF THE MODEL

In this analysis, we assumed a two-layer structure in air as schematically illustrated in Figure 23 to represent a typical bi-material pixel membrane. The bottom and top layers are air. In bi-material/microbolometer sensor applications, the supporting layer usually is a thin dielectric film of SiO_2 [17]. For this reason, next to the bottom layer there is a SiO_2 layer followed by a middle layer that can be any THz absorbing material. The index of refraction used for the dielectric material (SiO_2) was 1.46, whereas the index of refraction of the metal thin film is given by Equation (8).

The thickness of the SiO_2 layers was 1 μm as this is the thickness used for the bi-material structure in [17], while the thickness of the metal layer varied from 1 nm up to 150 nm. The range of the conductivities was from 10^4 S/m to 10^8 S/m. Note that the transmission, reflection and absorption coefficients of the bi-material structure were calculated for a single frequency of 2.85 THz at an angle of incidence of 30 degrees. However, the analysis can be easily extended to other frequencies as well as incident angles.

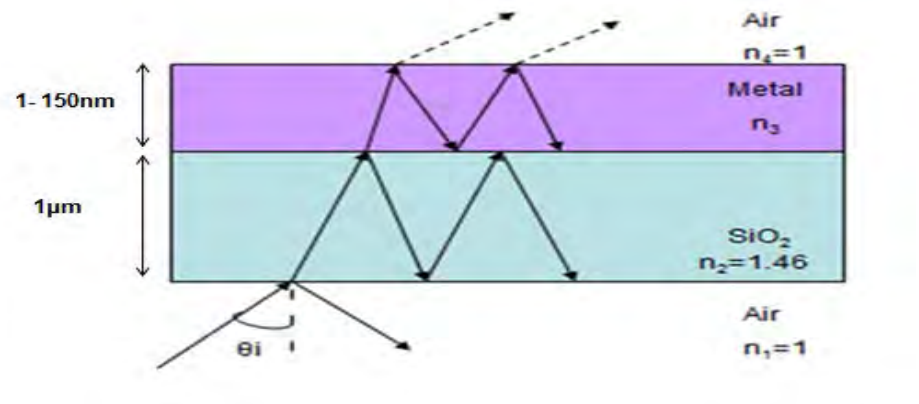

Figure 23. Four layer structure used for optimization of absorption.

The dependence of absorption on thickness and conductivity is shown in Figure 24. It can be seen in Figure 24 that for a given value of thickness, the absorption initially increases as conductivity decreases and then starts to fall. On the other hand, for a given value of conductivity, absorption increases as thickness decreases and then starts to decrease as the film gets thicker. It is interesting to find that the maximum absorption possible is 50% regardless of the conductivity and thickness [14].

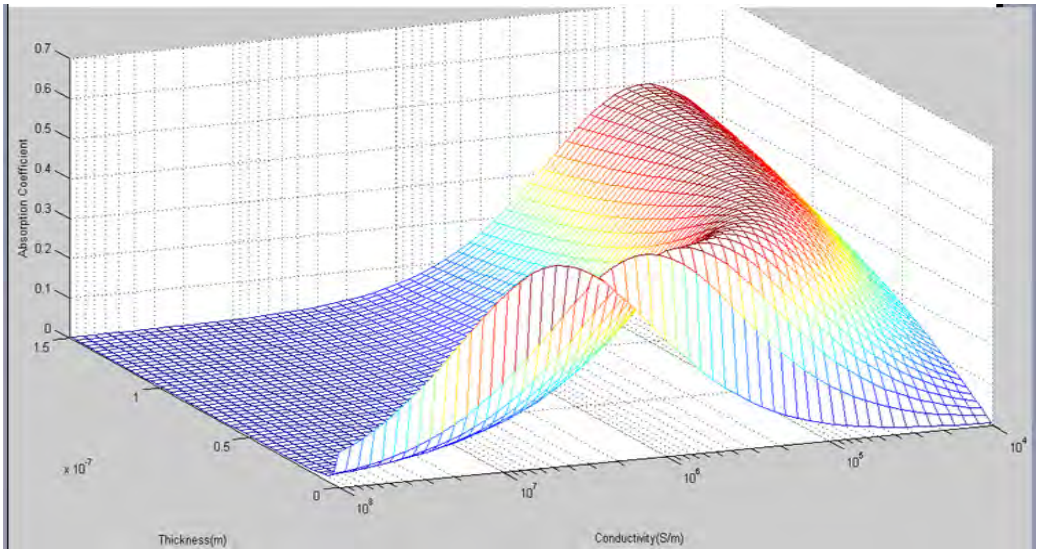

Figure 24. 3D plot of absorption a as a function of conductivity and thickness.

The comparison between the experimental values (black squares) and the model that was created is demonstrated in Figure 25. As expected, the experimental absorption data of nickel films follows the three-dimensional plot closely and reaches the red area where the maximum of 50% occurs. Note that thinner films are required for achieving maximum absorption when the conductivity of a film is higher. On the contrary, thicker films are needed for materials with lower conductivity to obtain maximum absorption [14].

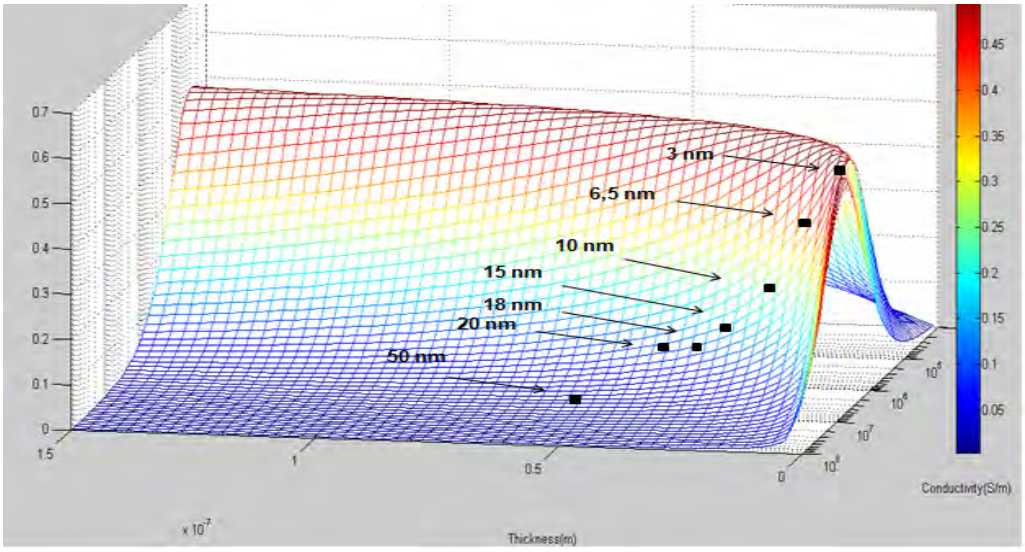

Figure 25. Experimental values of absorption for the Ni films superimposed on the 3D plot.

From the plot in Figure 26, we see the absorption as a function of Ni layer thickness in the 1 to 50 nm range. We can clearly observe that our experimental values, excluding the contribution from the substrate, follow the simulated dependence well. We also notice that absorption drops as thickness increases, which indicates that high absorption can be obtained only for the thin layers of Ni. It can also be seen that the optimum absorption occurs for a 2 to 3 nm thick Ni layer with absorption close to 50% [14].

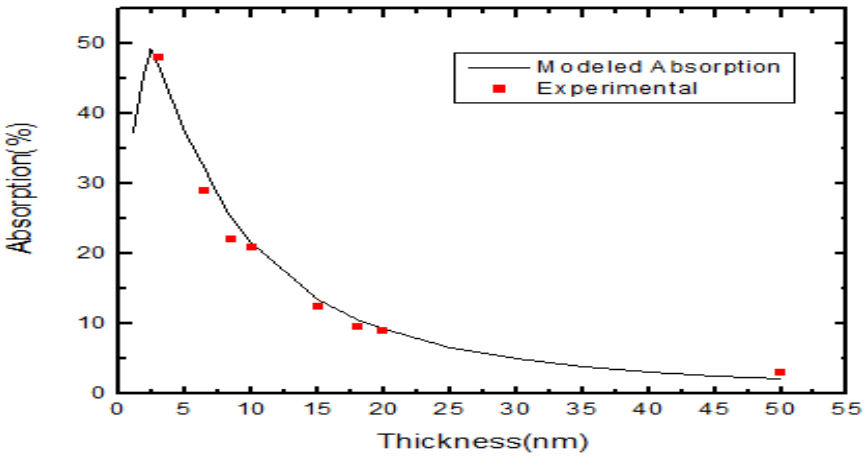

Figure 26. Measured and simulated absorption as a function of Ni film thickness without the substrate.

It should be taken into consideration that fabrication of such a thin Ni layers is relatively difficult. However, if a thicker film is employed, a substantially lower conductivity is needed, which excludes most metals. Alternatively, it is possible to use doped semiconductors, where the conductivity can be controlled in the range of 10^4 to 10^5 S/m (see Figure 27 showing the resistivity of doped Si), allowing the thickness of silicon layer to be in the 50–100 nm range [18].

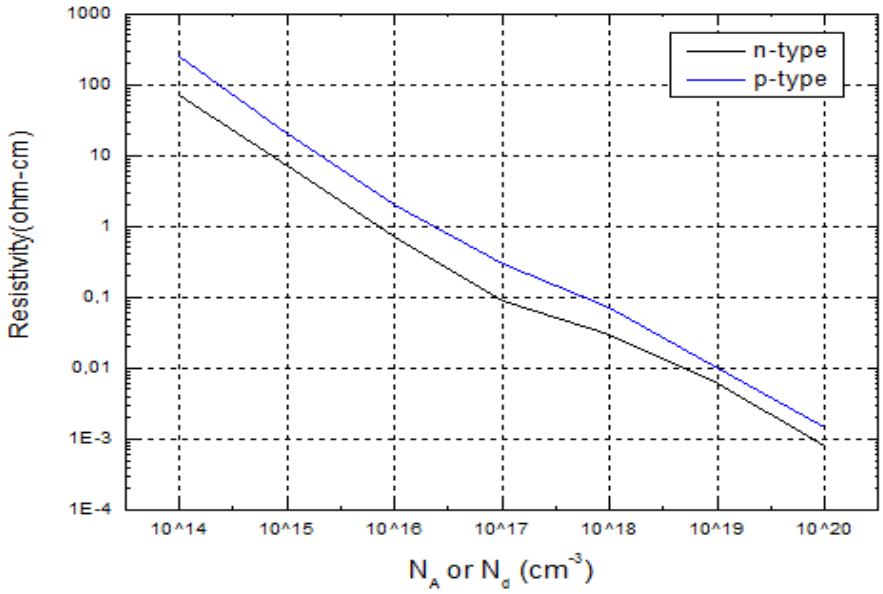

Figure 27. Resistivity versus impurity concentration at 300 K in silicon.

VI. SUMMARY, CONCLUSIONS AND FUTURE WORK

A. SUMMARY AND CONCLUSIONS

For improving the sensitivity of bi-material pixels for THz imaging applications, it is necessary to develop high THz absorbing thin films. In this thesis, nickel films with thickness ranging from 3 to 50 nm were characterized using Fourier transform infrared spectroscopy extended to the THz range. Experimental results show that nickel films can absorb up to 48% for frequencies between 2.5 and 10 THz depending on the thickness of the layer. It was found that the absorption increased from about 4% to 48 % when the film thickness was decreased from 50 to 3 nm. This happens because of the decrease in conductivity as the film thickness decreases resulting in higher Joule heating. Theoretical predictions of absorption show a good agreement with the experimental data, which validates our model. Our model can confidently predict the absorption of THz radiation in thin films depending on the thickness and conductivity. Further studies show that by decreasing the surface filling-factor of Ni, it is possible to increase absorption to the values obtained for the Cr films indicating that much lower stress Ni films can be used in bi-material MEMS detectors with absorption comparable with Cr films [14].

Further numerical analysis and model predictions allow the optimization of the sensitive layer properties and indicate that the maximum achievable value of absorption is 50% [14]. Moreover, simulation results show that by controlling the doping concentration and thickness, semiconductor films can be used instead of metal, making the design more flexible.

B. FUTURE WORK

As a future effort, meta-material structures can be designed for high THz absorbing with nearly 100% absorption at targeted frequencies [15]. Finally, these structures can be integrated with bi-material sensor pixels and fabricated using MEMS technology for achieving high sensitivity at specific THz frequencies. The optimized bi-

material sensors can be used for the fabrication of focal plane arrays that will lead to a highly sensitive THz camera for potential military and civilian applications.

APPENDIX A: MATLAB CODE DEVELOPED FOR CALCULATING THE TOTAL POWER REFLECTION OF THE NICKEL SAMPLES

```
                %Reflectance with substrate and 6.5nm Ni
d12=6.5e-9; d13=450e-6;

theta1=pi/6;
w=8300:50:53300;
lambda=1./w;
sigma_Ni4_3b=2777777.78;
sigma_Si4_3b=6.4e-4;
n12=(1-i).*5.47*sqrt(sigma_Ni4_3b*lambda);
n13=3.42-i.*(sigma_Si4_3b)*8.86*lambda;


theta2=asin(sin(theta1));theta3=asin(sin(theta1));theta4=asin(sin(theta1
));theta5=asin(sin(theta1));theta6=asin(sin(theta1));
theta7=asin(sin(theta1));theta8=asin(sin(theta1));theta9=asin(sin(theta1
));theta10=asin(sin(theta1));theta11=asin(sin(theta1));
theta12=asin(sin(theta1)./n12);theta13=asin(sin(theta1)./n13);theta14=as
in(sin(theta1));


phi2=2*pi./lambda*cos(theta2);phi3=2*pi./lambda*cos(theta3);phi4=2*pi./l
ambda*cos(theta4);phi5=2*pi./lambda*cos(theta5);
phi6=2*pi./lambda*cos(theta6);phi7=2*pi./lambda*cos(theta7);phi8=2*pi./l
ambda*cos(theta8);phi9=2*pi./lambda*cos(theta9);
phi10=2*pi./lambda*cos(theta10);phi11=2*pi./lambda*cos(theta11);phi12=2.
*pi./lambda.*n12.*d12.*cos(theta12);phi13=2.*pi./lambda.*n13.*d13.*cos(t
heta13);


r120=(cos(theta1)-cos(theta2))/(cos(theta1)+cos(theta2));
r23=(cos(theta2)-cos(theta3))/(cos(theta2)+cos(theta3));
r34=(cos(theta3)-cos(theta4))/(cos(theta3)+cos(theta4));
r45=(cos(theta4)-cos(theta5))/(cos(theta4)+cos(theta5));
r56=(cos(theta5)-cos(theta6))/(cos(theta5)+cos(theta6));
r67=(cos(theta6)-cos(theta7))/(cos(theta6)+cos(theta7));
r78=(cos(theta7)-cos(theta8))/(cos(theta7)+cos(theta8));
r89=(cos(theta8)-cos(theta9))/(cos(theta8)+cos(theta9));
r910=(cos(theta9)-cos(theta10))/(cos(theta9)+cos(theta10));
r1011=(cos(theta10)-cos(theta11))/(cos(theta10)+cos(theta11));
r1112=(cos(theta11)-
n12.*cos(theta12))./(cos(theta11)+n12.*cos(theta12));
r1213=(n12.*cos(theta12)-
n13.*cos(theta13))./(n12.*cos(theta12)+n13.*cos(theta13));
r1314=(n13.*cos(theta13)-
cos(theta14))./(n13.*cos(theta13)+cos(theta14));


r13=(r1213+r1314.*exp(-2i.*phi13))./(1+r1213.*r1314.*exp(-2i.*phi13));
```

```
r12=(r1112+r13.*exp(-2i.*phi12))./(1+r1112.*r13.*exp(-2i.*phi12));
r11=(r1011+r12.*exp(-2i.*phi11))./(1+r1011.*r12.*exp(-2i.*phi11));
r10=(r910+r11.*exp(-2i*phi10))./(1+r910*r11.*exp(-2i*phi10));
r9=(r89+r10.*exp(-2i*phi9))./(1+r89*r10.*exp(-2i*phi9));
r8=(r78+r9.*exp(-2i*phi8))./(1+r78*r9.*exp(-2i*phi8));r7=(r67+r8.*exp(-
2i*phi7))./(1+r67*r8.*exp(-2i*phi7));
r6=(r56+r7.*exp(-2i*phi6))./(1+r56*r7.*exp(-2i*phi6));r5=(r45+r6.*exp(-
2i*phi5))./(1+r45*r6.*exp(-2i*phi5));
r4=(r34+r5.*exp(-2i*phi4))./(1+r34*r5.*exp(-2i*phi4));r3=(r23+r4.*exp(-
2i*phi3))./(1+r23*r4.*exp(-2i*phi3));
r2=(r120+r3.*exp(-2i*phi2))./(1+r120*r3.*exp(-2i*phi2));



R2=r2.*conj(r2);

plot(w,R2)


fid = fopen('R--Nickel4_5.txt','wt');

for count = 1:500,
    fprintf(fid,'%6.8f  %12.8f\n',w(count),R2(count));
end
fclose(fid);
```

APPENDIX B: MATLAB CODE DEVELOPED FOR CALCULATING THE TOTAL POWER TRANSMISSION OF THE NICKEL SAMPLES

```
 % Transmittance with substrate and 6.5nm Ni no layers
d12=6.5e-9; d13=450e-6;

theta1=pi/6;
w=8300:50:53300;
lambda=1./w;
sigma_Ni4_3b=2777777.7;
sigma_Si4_3b=6.4e-4;
n12=(1-i).*5.47*sqrt(sigma_Ni4_3b*lambda);
n13=3.42-i.*(sigma_Si4_3b)*8.86*lambda;

theta2=asin(sin(theta1));theta3=asin(sin(theta1));theta4=asin(sin(theta1
));theta5=asin(sin(theta1));theta6=asin(sin(theta1));
theta7=asin(sin(theta1));theta8=asin(sin(theta1));theta9=asin(sin(theta1
));theta10=asin(sin(theta1));theta11=asin(sin(theta1));
theta12=asin(sin(theta1)./n12);theta13=asin(sin(theta1)./n13);theta14=as
in(sin(theta1));


phi2=2*pi./lambda*cos(theta2);phi3=2*pi./lambda*cos(theta3);phi4=2*pi./l
ambda*cos(theta4);phi5=2*pi./lambda*cos(theta5);
phi6=2*pi./lambda*cos(theta6);phi7=2*pi./lambda*cos(theta7);phi8=2*pi./l
ambda*cos(theta8);phi9=2*pi./lambda*cos(theta9);
phi10=2*pi./lambda*cos(theta10);phi11=2*pi./lambda*cos(theta11);phi12=2.
*pi./lambda.*n12.*d12.*cos(theta12);phi13=2*pi./lambda.*n13.*d13.*cos(th
eta13);


r120=(cos(theta1)-cos(theta2))/(cos(theta1)+cos(theta2));
r23=(cos(theta2)-cos(theta3))/(cos(theta2)+cos(theta3));
r34=(cos(theta3)-cos(theta4))/(cos(theta3)+cos(theta4));
r45=(cos(theta4)-cos(theta5))/(cos(theta4)+cos(theta5));
r56=(cos(theta5)-cos(theta6))/(cos(theta5)+cos(theta6));
r67=(cos(theta6)-cos(theta7))/(cos(theta6)+cos(theta7));
r78=(cos(theta7)-cos(theta8))/(cos(theta7)+cos(theta8));
r89=(cos(theta8)-cos(theta9))/(cos(theta8)+cos(theta9));
r910=(cos(theta9)-cos(theta10))/(cos(theta9)+cos(theta10));
r1011=(cos(theta10)-cos(theta11))/(cos(theta10)+cos(theta11));
r1112=(cos(theta11)-
n12.*cos(theta12))./(cos(theta11)+n12.*cos(theta12));
r1213=(n12.*cos(theta12)-
n13.*cos(theta13))./(n12.*cos(theta12)+n13.*cos(theta13));
r1314=(n13.*cos(theta13)-
cos(theta14))./(n13.*cos(theta13)+cos(theta14));


r13=(r1213+r1314.*exp(-2i.*phi13))./(1+r1213.*r1314.*exp(-2i.*phi13));
```

```
r12=(r1112+r13.*exp(-2i.*phi12))./(1+r1112.*r13.*exp(-2i.*phi12));
r11=(r1011+r12.*exp(-2i.*phi11))./(1+r1011.*r12.*exp(-2i.*phi11));
r10=(r910+r11.*exp(-2i*phi10))./(1+r910*r11.*exp(-2i*phi10));
r9=(r89+r10.*exp(-2i*phi9))./(1+r89*r10.*exp(-2i*phi9));
r8=(r78+r9.*exp(-2i*phi8))./(1+r78*r9.*exp(-2i*phi8));r7=(r67+r8.*exp(-
2i*phi7))./(1+r67*r8.*exp(-2i*phi7));
r6=(r56+r7.*exp(-2i*phi6))./(1+r56*r7.*exp(-2i*phi6));r5=(r45+r6.*exp(-
2i*phi5))./(1+r45*r6.*exp(-2i*phi5));
r4=(r34+r5.*exp(-2i*phi4))./(1+r34*r5.*exp(-2i*phi4));r3=(r23+r4.*exp(-
2i*phi3))./(1+r23*r4.*exp(-2i*phi3));
r2=(r120+r3.*exp(-2i*phi2))./(1+r120*r3.*exp(-2i*phi2));

t120=(2*cos(theta1))/(cos(theta1)+cos(theta2));
t23=(2*cos(theta2))/(cos(theta2)+cos(theta3));
t34=(2*cos(theta3))/(cos(theta3)+cos(theta4));
t45=(2*cos(theta4))/(cos(theta4)+cos(theta5));
t56=(2*cos(theta5))/(cos(theta5)+cos(theta6));
t67=(2*cos(theta6))/(cos(theta6)+cos(theta7));
t78=(2*cos(theta7))/(cos(theta7)+cos(theta8));
t89=(2*cos(theta8))/(cos(theta8)+cos(theta9));
t910=(2*cos(theta9))/(cos(theta9)+cos(theta10));
t1011=(2*cos(theta10))/(cos(theta10)+cos(theta11));
t1112=(2.*cos(theta11))./(cos(theta11)+n12.*cos(theta12));
t1213=(2.*n12.*cos(theta12))./(n12.*cos(theta12)+n13.*cos(theta13));
t1314=(2.*n13.*cos(theta13))./(n13.*cos(theta13)+cos(theta14));


t13=(t1213.*t1314.*exp(-i.*phi13))./(1+r1213.*r1314.*exp(-2i.*phi13));
t12=(t1112.*t13.*exp(-i.*phi12))./(1+r1112.*r13.*exp(-2i.*phi12));
t11=(t1011*t12.*exp(-i.*phi11))./(1+r1011*r12.*exp(-2i*phi11));
t10=(t910.*t11.*exp(-i.*phi10))./(1+r910.*r11.*exp(-2i.*phi10));
t9=(t89.*t10.*exp(-i.*phi9))./(1+r89.*r10.*exp(-2i.*phi9));
t8=(t78.*t9.*exp(-i.*phi8))./(1+r78.*r9.*exp(-2i.*phi8));
t7=(t67.*t8.*exp(-i.*phi7))./(1+r67.*r8.*exp(-2i.*phi7));
t6=(t56.*t7.*exp(-i.*phi6))./(1+r56*r7.*exp(-2i.*phi6));
t5=(t45.*t6.*exp(-i.*phi5))./(1+r45.*r6.*exp(-2i.*phi5));
t4=(t34.*t5.*exp(-i.*phi4))./(1+r34*r5.*exp(-2i.*phi4));
t3=(t23.*t4.*exp(-i.*phi3))./(1+r23.*r4.*exp(-2i.*phi3));
t2=(t120.*t3.*exp(-i.*phi2))./(1+r120*r3.*exp(-2i.*phi2));


T2=(cos(theta14)./(cos(theta1))).*t2.*conj(t2);


plot(w,T2);


fid = fopen('T--Nickel4_5.txt','wt');

for count = 1:500,
    fprintf(fid,'%6.8f  %12.8f\n',w(count),T2(count));
end
fclose(fid);
```

APPENDIX C: MATLAB CODE DEVELOPED FOR CALCULATING THE TOTAL ABSORPTION THROUGH A BI-MATERIAL STRUCTURE

```
%       Bi-Material structure
clear
clc

sigma_M=logspace(4,8,55);
d2=1e-6;
d3=1e-9:2.75e-9:150e-9;

n1=1;
n2=1.46;
n4=1;
theta1=pi/6;

lambda=1.05e-4;   % f=2.85 THz

n3=(1-i)*5.47*sqrt(sigma_M*lambda);   %n3= 1x55 index of refraction for
Ni
theta2=asin(n1*sin(theta1)/n2);
theta3=asin(n1*sin(theta1)./n3);  %theta3 is 1x55
theta4=asin(n1*sin(theta1)/n4);
phi2=(2*pi/lambda)*d2*n2*cos(theta2);

%loop for phi3


for k=1:55
    p= d3(k);
    phi3i=(2*pi/lambda)*p*n3.*cos(theta3);
phi3(k,:)=phi3i;                                %55x55

end


r120=(n1*cos(theta1)-n2*cos(theta2))/(n1*cos(theta1)+n2*cos(theta2));
r23=(n2*cos(theta2)-n3.*cos(theta3))./(n2*cos(theta2)+n3.*cos(theta3));
% r23=[1x55]
r34=(n3.*cos(theta3)-n4*cos(theta4))./(n3.*cos(theta3)+n4*cos(theta4));


for t=1:55
    P1=phi3(t,:);
    r3i=(r23+r34.*exp(-2i*P1))./(1+r23.*r34.*exp(-2i*P1));
    r3(t,:)=r3i;                                                %55x55


end
 r2=(r120+r3.*exp(-2i*phi2))./(1+r120.*r3.*exp(-2i*phi2));
```

```
       %55x55


t120=(2*n1*cos(theta1))/(n1*cos(theta1)+n2*cos(theta2));
t23=(2*n2*cos(theta2))./(n2*cos(theta2)+n3.*cos(theta3));
t34=(2*n3.*cos(theta3))./(n3.*cos(theta3)+n4*cos(theta4));

R2=r2.*conj(r2);    %55x55 ,TOTAL POWER REFLECTION COEFFICIENT %
%plot(w,R2);

for b=1:55
    K1=phi3(b,:);
    t3i=(t23.*t34.*exp(-i.*K1))./(1+r23.*r34.*exp(-2i.*K1));
    t3(b,:)=t3i;
       %t3= 55x55


end

 t2=(t120.*t3*exp(-i*phi2))./(1+r120*r3*exp(-2i*phi2));

  T2=(cos(theta4)/(cos(theta1))).*t2.*conj(t2);        %   TOTAL   POWER
TRANSMISSION COEFFICIENT %

A=1-(T2+R2)

[Xaxis,Yaxis]=meshgrid(d3,sigma_M);
mesh(Xaxis,Yaxis,transpose(A))
```

LIST OF REFERENCES

[1] P. Y. Han, G. C. Cho, and X.-C. Zhang, "Time-domain transillumination of biological tissues with terahertz pulses," *Opt. Lett.,* 25, p. 242–244, 2000.

[2] P. Bakopoulos et al., "A tunable Continuous Wave (CW) and Short-pulse Optical Source for THz Brain Imaging Applications," *Meas. Sci. Technol*, 20, 2009.

[3] G. Karunasiri, "Real Time THz Camera using microbolometer focal plane array," *7th International conference on Technology and the Mine Problem*, May 2–4, Monterey, CA, 2006.

[4] B. N. Behnken, G. Karunasiri, D. Chamberlin, and P. R. Robrish, "Real-time imaging using a 2.8 THz quantum cascade laser and uncooled infrared microbolometer camera," *Opt. Lett*., 33, 440–442, 2008.

[5] D. Grbovic and G. Karunasiri, "Fabrication of Bi-material MEMS detector arrays for THz imaging," *Proc. SPIE* 7311, 731108, 2009.

[6] D. Grbovic et al., "Arrays of SiO_2, substrate-free micromechanical uncooled infrared and THz detectors," *Journal of applied physics*, 104, 054508, 2008.

[7] C. Bolakis, "High terahertz absorbing nanoscale metal films for fabrication of micromechanical bi-material THz sensors," Naval Postgraduate School, Thesis, June 2010.

[8] C. Bolakis, D. Grbovic, N. V. Lavrik, and G. Karunasiri, "Design and characterization of terahertz-absorbing nano-laminates of dielectric and metal thin films," *Opt. Express,* 18, 14488–14495, 2010.

[9] C. C. Homes, *Fourier Transform Infrared Spectroscopy*, Brookhaven National Laboratory, Upton, NY, January 2007.

[10] *870 User's Guide*, Thermo Nicolet Corporation, Madison, 1999.

[11] P. Lecaruyer, E. Maillart, M. Canva, and J. Rolland, "Generalization of the Rouard Method to an Absorbing Thin-film Stack and Application to Surface Plasmon Resonance," *Appl. Opt.* 45(33), pp. 8419–8423, 2006.

[12] M. Born and E. Wolf, *Principles of Optics 7th edition (expanded)*. Cambridge University, 1999.

[13] J. I. Pankove, *Optical Processes in Semiconductors*. Dover, 1971.

[14] F. Alves, A. Karamitros, D. Grbovic, and G. Karunasiri, "Highly absorbing nano-scale metal films for terahertz," *SPIE Optics+Photonics*, San Diego, CA, 2011.

[15] D. Grbovic, F. Alves, A. Karamitros, B. Kearney, and G. Karunasiri, "Optimization of THz Absorption in Thin Metal Films," *accepted for IEEE Sensors*, Ireland, 2011.

[16] N. Laman, and D. Grischkowsky, "Terahertz Conductivity of Thin Metal Films," *Appl. Phys*., 93(5), p. 051105, 2008.

[17] D. Grbovic et al., "Arrays of SiO_2, substrate-free micromechanical uncooled infrared and THz detectors," *Journal of applied physics*, 104, 054508, 2008.

[18] S. M. Sze, *Physics of Semiconductor Devices*, 2nd ed. Wiley, New York, 1981.

INITIAL DISTRIBUTION LIST

1. Defense Technical Information Center
   Ft. Belvoir, Virginia

2. Dudley Knox Library
   Naval Postgraduate School
   Monterey, California

3. Graduate School of Engineering and Applied Sciences
   Naval Postgraduate School
   Monterey, California

4. Associate Professor Gamani Karunasiri
   Department of Physics
   Naval Postgraduate School
   Monterey, California

5. Associate Professor Dragoslav Grbovic
   Department of Physics
   Naval Postgraduate School
   Monterey, California

6. Associate Professor David Jenn
   Department of Electrical Engineering
   Naval Postgraduate School
   Monterey, California

7. Chairman Dan C. Boger
   Department of Information Science
   Naval Postgraduate School
   Monterey, California

8. Professor and Chairman Clark Robertson
   Department of Electrical Engineering
   Naval Postgraduate School
   Monterey, California

9. Apostolos Karamitros
   Naval Postgraduate School
   Monterey, California